Ultrasonics - Sonochemistry 40 (2018) 282–288

Contents lists available at ScienceDirect

Ultrasonics - Sonochemistry

journal homepage: www.elsevier.com/locate/ultson

# Ultrasound assisted synthesis of Ag-decorated $TiO_2$ active in visible light

M. Stucchi[a,b,*], C.L. Bianchi[b], C. Argirusis[c], V. Pifferi[b], B. Neppolian[d], G. Cerrato[e], D.C. Boffito[a]

[a] Polytechnique Montréal, Département de Génie Chimique, 2900 Edouard Montpetit Blvd, H3C 3A4 Montrèal (QC), Canada
[b] Università di Milano, Chemistry Department, Via Golgi 19, 20133 Milano, Italy
[c] National Technical University of Athens, School of Chemical Engineering, Athens, Greece
[d] SRM University, SRM Research Institute, Chennai, India
[e] Università di Torino & NIS Inter-departmental Centre, Torino, Italy

ARTICLE INFO

*Keywords:*
Ag-$TiO_2$
Ultrasound
One-step deposition
Ag nanoparticles
Visible light photocatalysis
Micrometric $TiO_2$

ABSTRACT

Titanium dioxide is the most popular photocatalyst to degrade organic pollutants in air, as well as in water. The principal drawback preventing its commercial application lies in its limited absorption of the visible light (400–700 nm), while it is active under UV irradiation (≤387 nm). Supporting noble metals in the form of nanoparticles on $TiO_2$ increases its activity in the visible range. However, both the synthesis of noble metal nanoparticles and their deposition on $TiO_2$ are multi-step processes that often require organic solvents. Here, we deposit Ag nanoparticles from $AgNO_3$ on the surface of micrometric $TiO_2$ with $H_2O$ as a solvent and under ultrasound irradiation at 30 W $cm^{-2}$. Ultrasound increases the surface amount of Ag on $TiO_2$ with heterogeneous size distribution of Ag nanoparticles, which are bigger and overlaid (1–20 nm vs. 0.5–3 nm) compared to the sample obtained in traditional conditions (TEM images). While this change in morphology had no effect on acetone photodegradation under UV light, the 5%, 10%, and 20% Ag-$TiO_2$ degraded 17%, 20% and 24% acetone under visible light, respectively. The 10% by weight Ag-$TiO_2$ sample obtained in absence of ultrasound only degraded 14% acetone in 6 h, while the bare $TiO_2$ was not active.

## 1. Introduction

Titanium dioxide photocatalysis emerged in the '80s as an approach to degrade water and air pollutants exploiting sunlight as a free energy source [1]. Light with energy greater than the band-gap of $TiO_2$ excites electrons from the valence band to the conduction band ($e_{CB}^-$), generating a positive hole in the valence band ($h_{VB}^+$). Part of these charged species migrate to the semiconductor surface and react with water to produce $^{\cdot}OH$ radicals [2], which oxidize organic pollutant to degradation intermediates, or, in the best scenario, they mineralize them [3]. Volatile organic compounds (VOCs) include hydrocarbons, ethers, ketons, aldehydes and, chloro-containing molecules among others. VOCs concentration is from 2 to 5 times higher in indoor environments compared to outdoors and may reach 1000 times the concentration at the background level outdoor after use of VOCs containing products, i.e., paints, cleansers, disinfectants, etc. [4].

The band gap of $TiO_2$ (3.2 eV) is such that only UV light (≤387 nm) provides sufficient energy for the electron transfer to the conduction band. Since ultraviolet light makes up only 4–5% of the solar spectrum and lighting in indoor environments emits in the visible range, the wide adoption of $TiO_2$ for photocatalytic applications is limited. Beside this aspect, electron-hole charge recombination is a major weakness as it reduces the overall quantum efficiency [5]. Noble metals like Ag, Au, Pt and Pd deposited on $TiO_2$ surface act as an electron trap [6], thus stabilizing the interfacial charge transfer [7], lowering the chances of $e^-/h^+$ recombination [8].

For example, Mohite et al. [9] prepared Au doped $TiO_2$ thin films by spray pyrolysis, decreasing the band gap and increasing the photoelectrocatalytic degradation of benzoic acid under UV light illumination of 49%. Even metal oxides such as $WO_3$ improve the photocatalytic activity of $TiO_2$ under solar light, as recently reported by Hunge et al. [10,11].

Seery and co-authors report Ag modified $TiO_2$ with increased visible light activity compared to bare $TiO_2$ [12] due to the surface plasmon band of Ag, which absorbs in the visible spectrum [13]. The scientific literature is rich of procedures and data on the synthesis of Ag NPs supported on $TiO_2$. Examples include impregnation from Ag colloidal dispersions [14] or from Ag inorganic salts [15,16], electrostatic self-assembly [17], and photo-reduction of Ag salts [18]. Only few manuscripts deal with the ultrasound-aided synthesis of supported Ag particles. Liu et al. synthesized nanofiber-supported Ag particles in the presence of different reducing agents, including short-chain alcohols

* Corresponding author at: Polytechnique Montréal, Département de Génie Chimique, 2900 Edouard Montpetit Blvd, H3C 3A4 Montrèal (QC), Canada.
*E-mail address:* marta.stucchi@polymtl.ca (M. Stucchi).

http://dx.doi.org/10.1016/j.ultsonch.2017.07.016
Received 8 June 2017; Received in revised form 8 July 2017; Accepted 8 July 2017
Available online 10 July 2017
1350-4177/ 

and nitrogen compounds [19]. Ye at al. deposited Ag seeds on the surface of $SiO_2/TiO_2$ core–shell composites in a multi-step process, growing them to the structure of Ag shells with formaldehyde as a solvent [20]. However, none of them specifies the ultrasound (US) operating conditions (e.g., power and frequency). Moreover, they both deposit Ag in the presence of organic solvents.

Sakkas et al. report the decoration of M- or MO-NPs by means of US in aqueous or organic solution containing dispersed ceramics or polymers in powder form [21].

US has a potential to impact every stage of the preparation of a material in liquid phase. US produces nanomaterials in amorphous state (due to the very high cooling rates) [22], or stabilizes crystalline phases [23] which is relevant to fields such as catalysis, magnetism and coating processes. US generates shock waves that facilitate coating and insertion/intercalation processes and improves the distribution of the active phase on a support [24]. The mechanical waves increase nucleation production rate (i.e., in the sol–gel process) and develop defects and deformations of solid surfaces, creating additional surface area and exposing active and selective catalytic sites [25]. Despite its undisputable advantages, US is a technique that is still unexplored in the synthesis of an enormous number of materials. Ultrasonic-synthesis may refer the manufacture of inorganic and organic materials or their deposition on supports, including metal oxides [21], and metallorganic compounds [26]. Other US-aided techniques comprise the modification of the structure and/or the morphology of already formed materials, for instance through the re-dispersion of the supported phase [27].

We recently made the choice to adopt micro-particles [28] because nanopowders exhibit potential risks in terms of dispersibility [29], ecotoxicity [30], persistency [31], and bioaccumulation [32]. The International Agency for Research on Cancer (IARC) classified ultrafine $TiO_2$ as possible carcinogenic to humans (IARC, 2010). Papers reporting synthesis of micrometric particles of $TiO_2$ are still few. Liu et al. reported the synthesis of porous $TiO_2$ microsphere [33]. However all the other data refer to sub-micrometric powders [34,35]. We first pioneered the photocatalytic application of commercial micrometric $TiO_2$ and proved that is as efficient as the nanometric $TiO_2$ [36,37]. Finally, in a recent work, we synthesized Cu NPs supported over micrometric $TiO_2$: while the bare micro-metric $TiO_2$ is inactive under visible light, the 40% by weight Cu-$TiO_2$ sample degrades 28% acetone in 6 h [38].

Here, we report the one-step US-assisted synthesis of Ag NPs. Our work is innovative for the following aspects: i) We are the first to report the ultrasonic synthesis of Ag-$TiO_2$ and we explicit US operating conditions; ii) Water is the solvent, which eliminates organic solvent disposal issues; iii) The support are micro-sized $TiO_2$ spheres as an alternative to nano-sized $TiO_2$, differently from the quasi-totality of the reported data.

The data reported in this manuscript show how the photocatalytic activity under visible light increases for the samples obtained with ultrasound.

## 2. Experimental

### 2.1. Materials

The support was $TiO_2$ (1077, KRONOS Worldwide, Inc.), which is pure anatase as of its crystallographic structure. We characterized it in a previous work [37], and here we summarized the main features (Table 1).

**Table 1**
$TiO_2$ (1077, KRONOS Worldwide, Inc.) features.

| BET surface area ($m^2\,g^{-1}$) | Particle size range (nm) | XPS Ti $2p_{3/2}$ (eV) | XPS $OH/O_{tot}$ | Band gap (eV) |
|---|---|---|---|---|
| 12 ± 2 $m^2\,g^{-1}$ | 110–130 | 458.4 | 0.32 | 3.15 |

Silver nitrate ($AgNO_3$, ACS Reagent, ≥99%) was the metal precursor. The other reagents were polyvinylpyrrolidone (PVP40, average mol wt 40,000) and sodium borohydride ($NaBH_4$, ≥99%). The model compound for the photocatalytic degradation tests was acetone (CHROMASOLV® Plus, for HPLC, ≥99.9%).

### 2.2. Synthesis of Ag-$TiO_2$

We followed the synthesis reported by Goharshadi et al. [39] to decorate the micro-sized $TiO_2$ with Ag nanoparticles (NPs). The precursor solutions were two: the first solution contained $AgNO_3$, polyvinyl pyrrolidone (PVP40, surfactant) in the amount of 0.02 g, $TiO_2$ 1077, while the second was a $NaBH_4$ 0.1 M. aqueous solution. $AgNO_3$ ranged from 0.02 g to 0.4 g, depending on the sample. The amount of $TiO_2$ was fixed at 2 g.

Ultrasound (US) irradiated the first solution for 10 min before the $NaBH_4$ solution was added in 2 min. Afterwards, the sonication was maintained for 60 min at the same power.

$Ag(^0)$ forms with the following reaction: $AgNO_3 + NaBH_4 + 3H_2O \rightarrow Ag + H_3BO_3 + NaNO_3 + 7/2\ H_2$.

The finished powder was washed with distilled water 3 times, dried at 100 °C for 24 h, and calcined in static air at 400 °C, for 2 h.

We recently published a work on the ultrasound synthesis of Cu NPs supported on $TiO_2$, whereby Cu ranged from 1% to 20% [38]. In the present work, we made the choice of optimizing the Ag loading in the same range.

The US processor was a Bandelin SONOPLUS HD 3200 ultrasound generator with a nominal power of 200 W, equipped with a sonication horn (fixed frequency: 20 kHz). The horn tip diameter was 13 mm, thus resulting in a power of 30 W $cm^{-2}$.

### 2.3. Catalyst characterization

The surface area of all the catalysts was measured by conventional $N_2$ adsorption (BET) at 77 K using a Sorptometer (Costech Mod. 1042).

A PW 3830/3020 X' Pert Diffractometer from PANalytical working Bragg-Brentano with the Cu Kα1 radiation (k = 1.5406 Å) analyzed the crystallographic composition. High-resolution transmission electron microscopy (HR-TEM, JEOL 3010-UHR Instrument, acceleration potential 300 kV, LaB6 filament) surveyed the surface of the particles. A Thermo Scientific Evolution 600 spectrophotometer equipped with a diffuse reflectance accessory Praying-Mantis sampling kit measured the absorbance, (Harrick Scientific Products, USA). The reference material was a Spectralon1 disk. The Kubelka–Munk function originated the plot of the experimental absorption versus the wavelength [40]. A M-probe spectrophotometer (Surface Science Instruments) measured the X-ray photoelectron spectra (XPS) absorbance. The source was a monochromatic Al Kα radiation (1486.6 eV). The accuracy of the reported binding energy (BE) can be estimated at ± 0.2 eV. A Perkin Elmer Optima 8300 instrument carried out the ICP/OES analysis. The samples were first mineralized by nitric acid followed by microwave treatment.

### 2.4. Reactor design and photocatalytic tests

UV and visible light irradiated the samples to promote the degradation of acetone as a model compound. The setup for the photocatalytic tests consisted of a PIREX glass reactor (5 L volume), connected to a micro-gaschromatograph (Agilent 3000 A microGC), which quantified the acetone in the gas phase (Fig. 1).

The catalyst was in the form of a thin film deposited on a 100 $cm^2$ glass slab (Fig. 2) [41].

The film was deposited as follows: 50 mg of powder were suspended in 10 ml of isopropanol. Three layers of the suspension were deposited on the glass slab before each test and let dry. The source of light was an UV lamp (Jelosil–Model HG-500, 500 W, k = 315–400 nm) or LED (MW mean well, 350 mA rated current, 9–48 V DC voltage range,

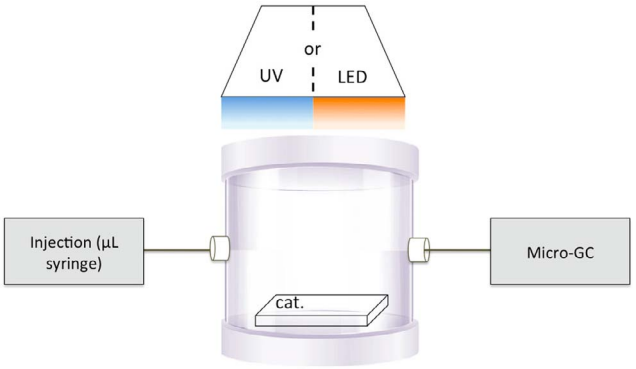


**Fig. 1.** Setup scheme.

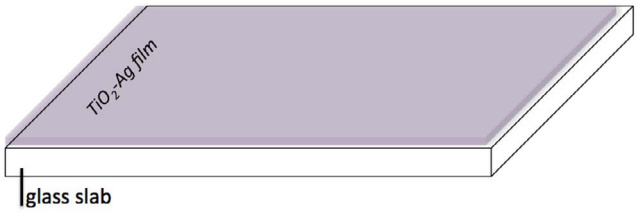


**Fig. 2.** $TiO_2$ catalyst deposited on glass slab.

16.8 W rated power) with light emission between 400 nm and 700 nm. A radiometer measured the irradiation power at the catalyst surface, so as to position the lamps at a distance resulting in an emission of 30 W $cm^{-2}$ for UV and 15,000 lux for LED.

## 3. Results and discussion

### 3.1. Surface area and HR-TEM imaging

Surface area of bare $TiO_2$ was 12 ± 2 $m^2 g^{-1}$ and this value remained unchanged for all the samples decorated with Ag.

The HR-TEM imaging provides information on the particle size and distribution of Ag over $TiO_2$. The micro-sized dimension of $TiO_2$ is unchanged after ultrasound (US) treatment (Fig. 3). US does not therefore affect the morphology of the support, without significant surface erosion. The main crystallographic family of planes observed is the (1 0 1) belonging to the anatase polymorph (Ref. ICDD anatase file No. 21-1272). US does modify the silver NPs morphology on the $TiO_2$ surface. Deposition of Ag by the traditional method (Fig. 3C) resulted in a fine distribution of nano-disperse particles, ranging from 0.5 to 3 nm. Instead of increasing the dispersion, US had rather an effect on the amount of Ag loaded. US provoked the growth of Ag crystallites over the surface of $TiO_2$ in the form of aggregates. The overlapped Ag NPs, thus expanded in different dimensional ranges, from 1 to 20 nm (Fig. 3A and B). This is ascribable to the increased diffusion rate of the solute [23,42]. Moreover, the analysis of the fringe patterns that sometimes are evident, are ascribable to the (1 1 1) family of metallic Ag on the basis of the dhkl distances (Ref. ICDD file No. 004-0783)

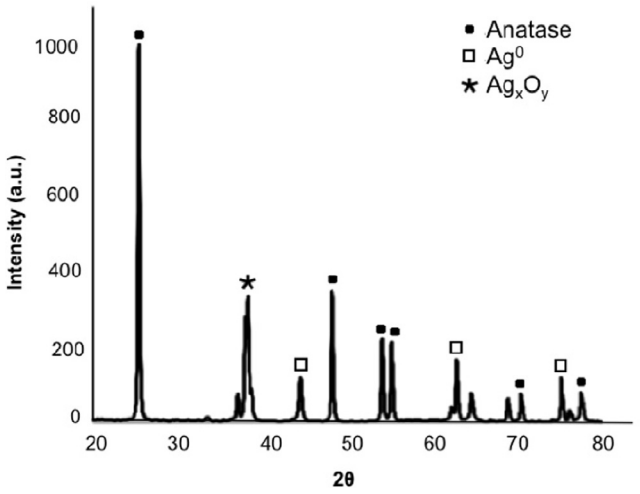


**Fig. 4.** XRD spectrum of Ag-$TiO_2$ 10% synthesized by ultrasound.

(Fig. 3A and B). The improved mass transfer between PVP and silver under the action of the mechanical waves facilitates the adsorption of Ag NPs onto the $TiO_2$ surface, resulting in the heterogeneity of the Ag NPs distribution on $TiO_2$ [43].

### 3.2. Crystallographic phase composition and XPS analysis

We reported the spectrum of 10% by weight Ag-$TiO_2$ as a representative for the Ag-$TiO_2$ samples (Fig. 4). If decorated on the surface with Ag, the sample maintains the typical crystallographic phase composition of $TiO_2$ anatase, as reported by Bianchi et al. [36]. Peaks at 25° and 48° 2θ correspond to $TiO_2$ in the anatase phase (JCPDS No.: 88-1175 and 84-1286). Peaks at 2θ of 65°, 78°, 45° confirm the presence of metallic Ag, while the peak at a 2θ of 38° reveals the presence of $Ag_2O$, ascribable to the oxidation of Ag during the calcination.

For $Ag_2O$ and AgO the shifts are approximately −0.3 eV and −0.8 eV due to initial-state factors of ionic charge and lattice potential [45]. Thus, both binding energies for $Ag_2O$ and AgO are similar (Table 2). XPS survey analysis (Fig. 5) confirmed the presence of both Ag in metal and metal-oxide form, as expected after the calcination. Mostly $Ag_2O$ contributes to increase the visible light absorption [46].

ICP analysis confirmed the % of Ag amount with an error < 2%.

### 3.3. UV–Vis absorption and band gap quantification

US mainly affected the size of Ag nanoparticles on $TiO_2$ surface (Fig. 3). UV–Vis spectra proved that this is the crucial feature to increase the adsorption at wavelengths in the visible range of 400 nm and 700 nm (Fig. 6).

Generally, noble metal nanostructures exhibit strong light absorption behavior due to the surface plasmon resonance (SPR) derived from the collective oscillation of surface electrons [47]. Several papers report the effect of Ag NPs on the Vis range light absorption [48], the improvement of the efficiency of thin film C—Si solar cell [49], or the light

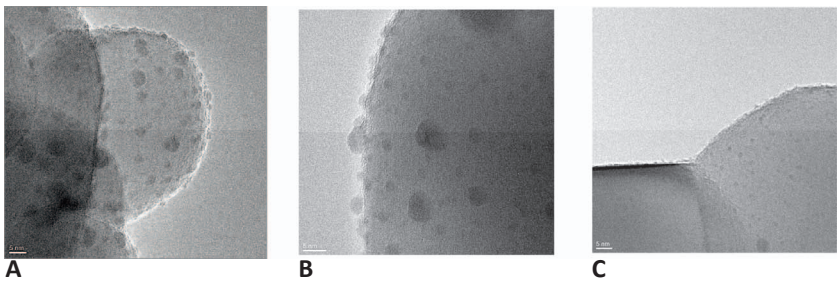


**Fig. 3.** HR-TEM images of $TiO_2$ decorated with Ag NPs (10%) with (A, B) and without (C) US.

**Table 2**
XPS binding energy (eV) of metal and metal-oxides Ag from handbook [44].

| Silver – Ag<br>$3d_{5/2}$ = 368.2 eV<br>Δ = 6.0 eV | | |
|---|---|---|
| | Oxidation state | Binding energy (eV) |
| Ag-$TiO_2$ | $Ag^{2+}$ (AgO); $Ag^{+}$ ($Ag_2O$) | 367.6 ( ± 0.8) eV |

absorption enhancement of polymeric films [50], confirming that localized plasmonic resonances can be used as efficient light trapping region of Ag-$TiO_2$.

We observed a slight, but still significant reduction of the band gap. The UV–VIS absorption spectra were e-elaborated with the Kubelka Munk function (Fig. 7). Tangent line crosses x-axis at the band gap values, at 3.1 eV–3.2 eV. The band gap decreases mainly because of the electronic defects introduced by Ag. Ag nanoparticles on $TiO_2$ are able to capture the electrons of the visible light, making them usable in the redox reactions that occur upon the surface. Both metal and metal oxides are able to act as an electron trap, reducing the electron-hole recombination rate [51].

The so-called “antenna mechanism” refers to the electrons or holes transfer between some particles in contact; the particle on the semiconductor surface act as much as electron traps as hole traps, and the immediate effect is a better electron-hole separation [52].

This passage of electrons, assumed in the M-$TiO_2$ systems described in this paper, takes place thanks to the differences between the valence and conduction bands of the respective elements [53,54]. The band gap of $Ag_xO_y$ species ranges from 1.69 to 1.71 eV [55]. According to relative energy band positions between $TiO_2$ and visible-light-absorbing semiconductors, the coupling between Ag and $TiO_2$ forms an heterojunction.

### 3.4. Photocatalytic activity

Photolysis is negligible being acetone concentration constant in time (Fig. 8). Error bars ( ± 5%) refer to the instrument resolution and their overlap is consistent with the oscillation of the concentrations.

The commercial $TiO_2$ (Kronos) degrades acetone when irradiated by UV light according to the following oxidation pathway:

$$C_3H_6\ O \rightarrow C_2H_4\ O \rightarrow CH_2\ O + CH_3COOH + CO_2 \rightarrow CH_2O_2 + CO_2 \rightarrow CO_2$$

After 90 min, 100% acetone was mineralized [37].

In this case, we did not observe any photocatalytic activity under visible light up to 5% of Ag loading (Table 3). The modification of Ag NPs morphology due to US application (see TEM, Fig. 3) does not have an impact on the degradation rate of acetone: the 10% by weight sample synthesized with US degrades acetone at the same rate as the

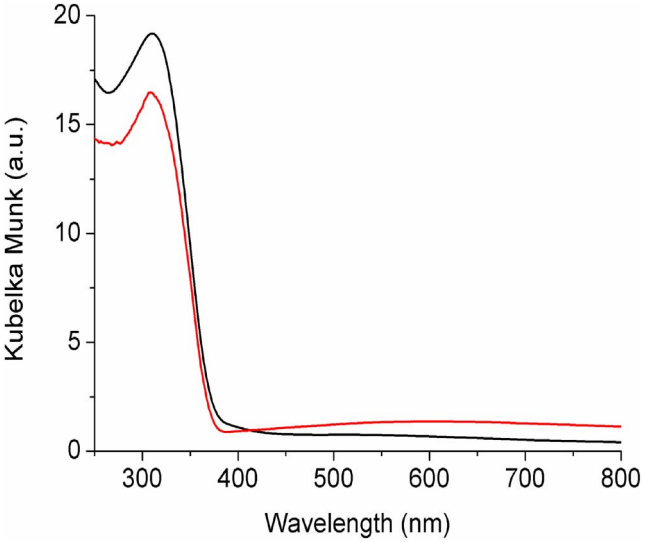


**Fig. 6.** Absorbance spectra in UV–VIS region of $TiO_2$ decorated with Ag NPs (10%) with (red line) and without (black line) US. (For interpretation of the references to colour in this figure legend, the reader is referred to the web version of this article.)

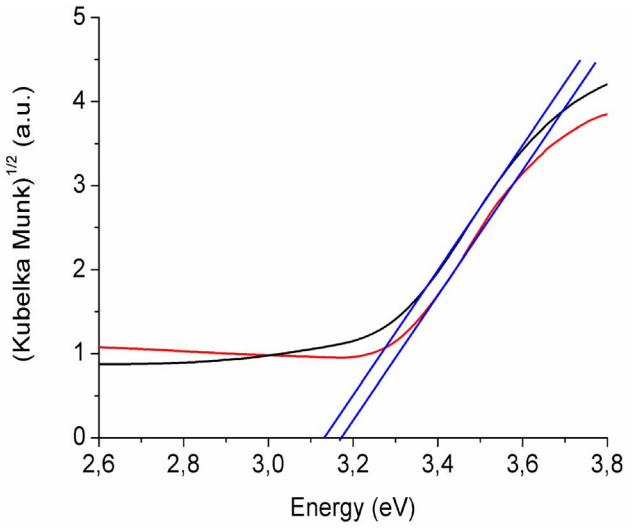


**Fig. 7.** KM1/2 vs. photon energy (eV) of $TiO_2$ decorated with Ag NPs (10%) with (red line) and without (black line) US. Tangent lines (blue) intercept the band gap values on x-axis. (For interpretation of the references to colour in this figure legend, the reader is referred to the web version of this article.)

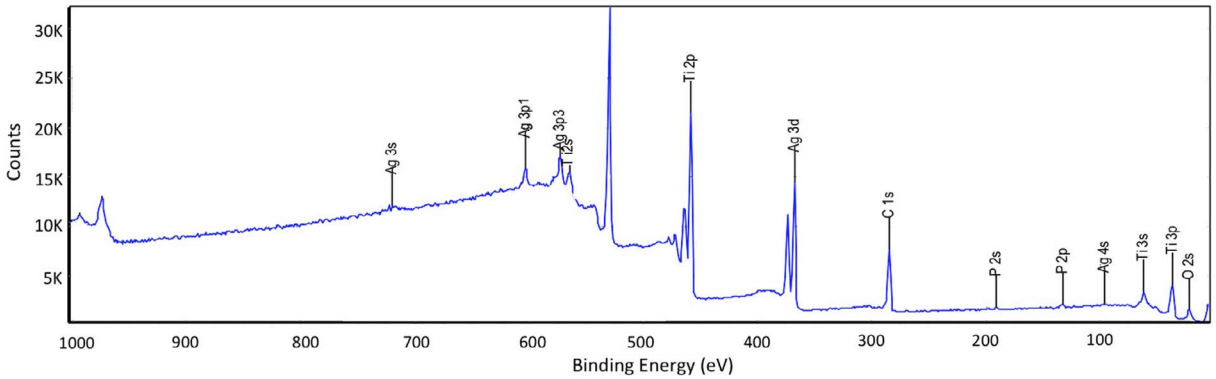


**Fig. 5.** XPS survey analysis of Ag decorated $TiO_2$.

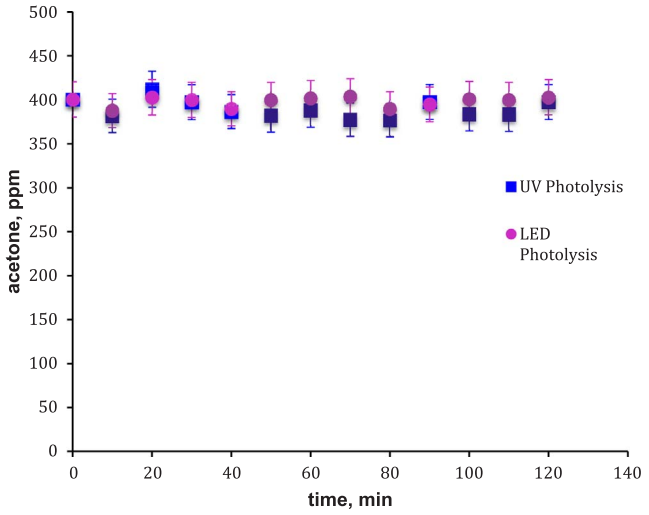


**Fig. 8.** UV and LED photolysis of acetone.

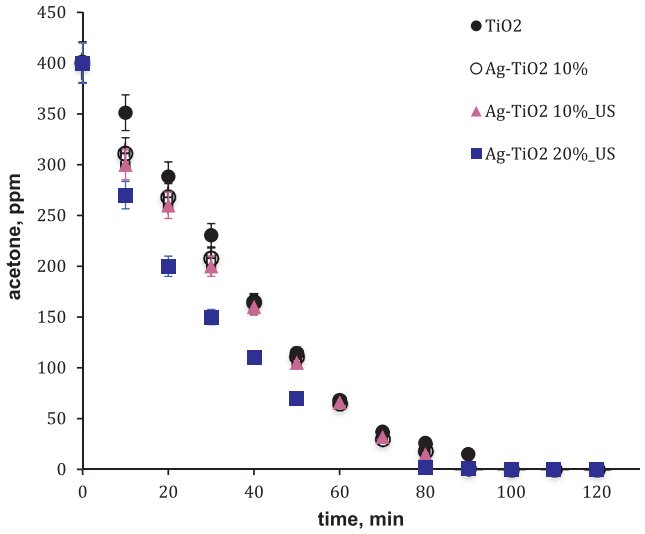


**Fig. 9.** Acetone photodegradation under UV-A irradiation (30 W $cm^{-2}$). Comparison between bare $TiO_2$ (black dots) and $TiO_2$ decorated with Ag NPs without US (empty dots) or by US (10–20 Ag%). Error bars refer to instrument resolution.

sample obtained with traditional impregnation (Fig. 9). Differently, the 20% by weight Ag-$TiO_2$ sample completely degrades acetone in 20 min. This is ascribable to higher loading of Ag. The presence of Ag on the surface decreases the band gap (Fig. 7), thus the number of electrons that can be potentially promoted from the valence to the conduction band increases. On the other hand, a shorter band gap increases the $e^-/h^+$ recombination rate, which is unfavorable. However, according to our experimental data, the increased electron absorption seems not only to annul, but to overcome this drawback. For what concerns UV photodegradation the improvement in the photodegradation of organics is evident in terms of the reduced time to achieve the complete mineralization (Fig. 9).

Photodegradation under LED as the only source of light is in line with the characterization results. The almost absent activity of naked $TiO_2$ is indeed ascribable to its wide band gap of 3.2 eV. Visible light is in this case insufficient to excite electrons from the valence band to the conduction band (Fig. 10). Ag decoration introduces a tremendous improvement. Ag nanoparticles absorb visible light due to the plasmonic resonance; moreover, by settling on the $TiO_2$ surface they create a junction permitting the electron transfer from Ag to $TiO_2$. The number of electrons available at the surfaces therefore increases. As a consequence, the concentration of photo-generated species ($^{\cdot}OH$ and $O_2^{\cdot -}$) at the $TiO_2$ surfaces is higher and the oxidation and reduction more likely to occur. Ag-$TiO_2$ absorbs beyond 400 nm (black line, Fig. 3), hence also the electrons of $TiO_2$ gain photo-energy because of the accumulative higher light absorption capacity. Moreover, Ag acts also as an electron sink, and this is the reason why the wider dimensions range of Ag nanoparticles play a crucial role, together with the Ag amount (Fig. 10).

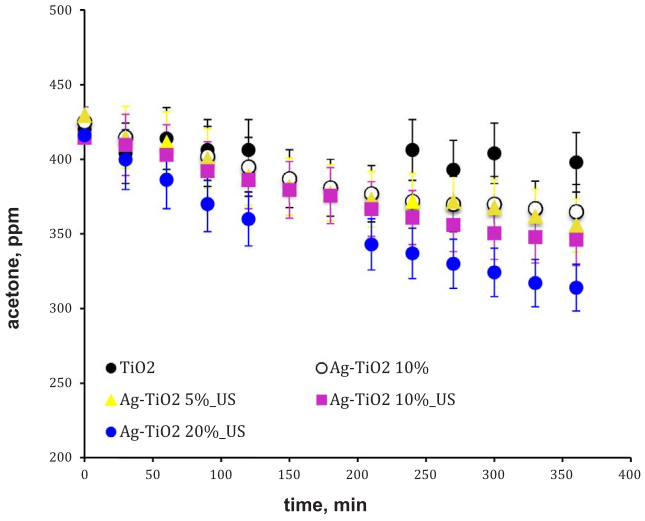


**Fig. 10.** Acetone photodegradation under LED irradiation using bare $TiO_2$ (black dots) or $TiO_2$ decorated with Ag NPs without US (white dots) or with US in the range 5–20%.

## 4. Conclusion

We deposited 1–20% by weight of Ag on micro-metric $TiO_2$ in one step either in presence of ultrasound or by traditional impregnation. We tested the photocatalysts in the degradation of acetone as a model compound under UV and visible light.

Under the tested conditions of 30 W $cm^{-2}$ for 70 min, ultrasound increases the Ag surface loading on $TiO_2$ by acting on the size of Ag crystallites, which are heterogeneous compared to the traditional impregnation: Ag aggregates ranged from 1 to 2 nm vs. 0.3 to 3 nm.

Ultrasound increases the Ag surface loading on $TiO_2$ by acting on the size of Ag crystallites, which are heterogeneous compared to the traditional impregnation: Ag aggregates ranged from 1 to 2 nm vs. 0.3 to 3 nm.

While the degradation of acetone under UV light only depended on the Ag loading and was the highest for the 20% by weight Ag-$TiO_2$

**Table 3**
Acetone degradation rates for photocatalytic reactions by UV (first column) and LED (second column).

| Sample | Acetone degradation rate (mg $m^{-3}$ $min^{-1}$) – UV irradiation | Acetone degradation rate (mg $m^{-3}$ $min^{-1}$) – LED irradiation |
|---|---|---|
| $TiO_2$ | 7.92 mg $m^{-3}$ $min^{-1}$ | 0 mg $m^{-3}$ $min^{-1}$ |
| Ag-$TiO_2$ 10% | 7.92 mg $m^{-3}$ $min^{-1}$ | 0.23 mg $m^{-3}$ $min^{-1}$ |
| Ag-$TiO_2$ 5% | – | 0.29 mg $m^{-3}$ $min^{-1}$ |
| Ag-$TiO_2$ 10%_US | 9.50 mg $m^{-3}$ $min^{-1}$ | 0.36 mg $m^{-3}$ $min^{-1}$ |
| Ag-$TiO_2$ 20%_US | 10.56 mg $m^{-3}$ $min^{-1}$ | 0.57 mg $m^{-3}$ $min^{-1}$ |

sample, under visible light the samples obtained with ultrasound were more active. In 6 h they degraded 3–11% more acetone compared to the samples synthesized with traditional impregnation in 6 h.

The advantages of micro-metric $TiO_2$ over nano-metric $TiO_2$ are several. Micro-metric $TiO_2$ (e.g., Kronos $TiO_2$) costs 10 times less than the nano-metric P25. Moreover, micro-metric $TiO_2$ is safer than nano-metric powders, because it eliminates the health risks related to inhalation.

Therefore, Ag deposited over micrometric $TiO_2$ is a viable and safer alternative to the nano-metric TiO2 as a photocatalyst. Moreover, Ag makes it active under visible light.

## References


[1] M. Pelaez, N.T. Nolan, S.C. Pillai, M.K. Seery, P. Falaras, A.G. Kontos, P.S.M. Dunlop, J.W.J. Hamilton, J.A. Byrne, K. O'Shea, M.H. Entezari, D.D. Dionysiou, A review on the visible light active titanium dioxide photocatalysts for environmental applications, Appl. Catal. B 125 (2012) 331–349.

[2] P.D. Cozzoli, R. Comparelli, E. Fanizza, M.L. Curri, A. Agostiano, Photocatalytic activity of organic-capped anatase $TiO_2$ nanocrystals in homogeneous organic solutions, Mater. Sci. Eng. C 23 (2003) 707–713.

[3] A.J. Hoffman, E.R. Carraway, M.R. Hoffmann, Photocatalytic production of $H_2O_2$ and organic peroxides on quantum-sized semiconductor colloids, Environ. Sci. Technol. 28 (5) (1994) 776–785.

[4] www.epa.gov, Volatile Organic Compounds' Impact on Indoor Air Quality.

[5] W. Choi, A. Termin, M.R. Hoffmann, The role of metal ion dopants in quantum-Sized $TiO_2$: correlation between photoreactivity and charge carrier recombination dynamics, J. Phys. Chem. 98 (51) (1994) 13669–13679.

[6] X.Z. Li, F.B. Li, Study of Au/$Au^{3+}$-$TiO_2$ photocatalysts toward visible photooxidation for water and wastewater treatment, Environ. Sci. Technol. 35 (11) (2001) 2381–2387.

[7] D. Behar, J. Rabani, Kinetics of hydrogen production upon reduction of aqueous $TiO_2$ nanoparticles catalyzed by $Pd^0$, $Pt^0$, or $Au^0$ coatings and an unusual hydrogen abstraction; steady state and pulse radiolysis study, J. Phys. Chem. B 110 (2006) 8750–8755.

[8] W. Wang, J. Zhang, F. Chen, D. He, M. Anpo, Preparation and photocatalytic properties of $Fe^{3+}$-doped Ag@$TiO_2$ core–shell nanoparticles, J. Colloid Interfaces Sci. 323 (2008) 182–186.

[9] V.S. Mohite, M.A. Mahadik, S.S. Kumbhar, Y.M. Hunge, J.H. Kim, A.V. Moholkar, K.Y. Rajpure, C.H. Bhosale, Photoelectrocatalytic degradation of benzoic acid using Au doped $TiO_2$ thin films, J. Photochem. Photobiol. B 142 (2015) 204–211.

[10] Y.M. Hunge, M.A. Mahadik, A.V. Moholkar, C.H. Bhosale, Photoelectrocatalytic degradation of oxalic acid using $WO_3$ and stratified $WO_3$/$TiO_2$ photocatalysts under sunlight illumination, Ultrason. Sonochem. 35 (2017) 233–242.

[11] Y.M. Hunge, Sunlight assisted photoelectrocatalytic degradation of benzoic acid using stratified $WO_3$/$TiO_2$ thin films, Ceram. Int. 43 (2017) 10089–10096.

[12] M.K. Seery, R. George, P. Floris, S.C. Pillai, Silver doped titanium dioxide nanomaterials for enhanced visible light photocatalysis, J. Photochem. Photobiol. A 189 (2007) 258–263.

[13] T.N. Nolan, M.K. Seery, S.J. Hinder, L.F. Healy, S.C. Pillai, A systematic study of the effect of silver on the chelation of formic acid to a titanium precursor and the resulting effect on the anatase to rutile transformation of $TiO_2$, J. Phys. Chem. C 114 (2010) 13026–13034.

[14] A. Yu, Q. Wang, J. Wang, C. Chang, Rapid synthesis of colloidal silver triangular nanoprisms and their promotion of $TiO_2$ photocatalysis on methylene blue under visible light, Catal. Commun. 90 (2017) 75–78.

[15] Y. Cui, Q. Ma, X. Deng, Q. Meng, X. Cheng, M. Xie, X. Li, Q. Cheng, H. Liu, Fabrication of Ag-$Ag_2O$/reduced $TiO_2$ nanophotocatalyst and its enhanced visible light driven photocatalytic performance for degradation of diclofenac solution, Appl. Catal. B 206 (2017) 136–145.

[16] T.T. Wang, P. Raghunath, Y.G. Lin, M.C. Lin, Synergistic effect of hydrogenation and thiocyanate treatments on Ag-Loaded $TiO_2$ nanoparticles for solar-to-hydrogen conversion, J. Phys. Chem. C 121 (2017) 9681–9690.

[17] Y. Li, P. Wang, C. Huang, W. Yao, Q. Wu, Q. Xu, Synthesis and photocatalytic activity of ultrafine $Ag_3PO_4$ nanoparticles on oxygen vacated $TiO_2$, Appl. Catal. B: Environ. 205 (2017) 489–497.

[18] P.V. Viet, B.T. Phan, C.M. Thi, L.V. Hieu, Controlled formation of silver nanoparticles on $TiO_2$ nanotubes by photoreduction method, J. Nanosci. Nanotechnol. 16 (2016) 1–7.

[19] K.G. Liu, A.R. Abbasi, A. Azadbakht, M.L. Hu, A. Morsali, Deposition of silver nanoparticles on polyester fiber under ultrasound irradiations, Ultrason. Sonochem. 34 (2017) 13–18.

[20] X. Ye, S. Cai, C. Zheng, X. Xiao, N. Hua, Y. Huang, $SiO_2$/$TiO_2$/Ag multilayered microspheres: preparation, characterization, and enhanced infrared radiation property, Appl. Surf. Sci. 345 (2015) 279–285.

[21] P.M. Sakkas, O. Schneider, G. Sourkouni, C. Argirusis, Sonochemistry in the service of SOFC research, Ultrason. Sonochem. 21 (2014) 1939–1947.

[22] A. Gedanken, Using sonochemistry for the fabrication of nanomaterials, Ultrason. Sonochem. 11 (2004) 47–55.

[23] D.C. Boffito, V. Crocellà, C. Pirola, B. Neppolian, G. Cerrato, M. Ashokkumar, Ultrasonic enhancement of the acidity, surface area and free fatty acids esterification catalytic activity of sulphated $ZrO_2$–$TiO_2$ systems, J. Catal. 297 (2013) 17–26.

[24] V. Belova, D.A. Gorin, D.G. Shchukin, H. Mohwald, Controlled effect of ultrasonic cavitation on hydrophobic/hydrophilic surfaces, Mater. Interfaces 3 (2) (2011) 417–425.

[25] A. Comazzi, C. Pirola, M. Longhi, C.L. Bianchi, K.S. Suslick, Fe-based heterogeneous catalysts for the Fischer-Tropsch reaction: sonochemical synthesis and bench-scale experimental tests, Ultrason. Sonochem. 34 (2017) 774–780.

[26] A. Maleki, M. Aghaei, H.R. Hafizi-Atabak, M. Ferdowsi, Ultrasonic treatment of $CoFe_2O_4$@$B_2O_3$-$SiO_2$ as a new hybrid magnetic composite nanostructure and catalytic application in the synthesis of dihydroquinazolinones, Ultrason. Sonochem. 37 (2017) 260–266.

[27] C. Pirola, C.L. Bianchi, A. Di Michele, P. Diodati, D.C. Boffito, V. Ragaini, Ultrasound and microwave assisted synthesis of high loading Fe-supported Fischer Tropsch catalysts, Ultrason. Sonochem. 17 (2010) 610–616.

[28] M. Stucchi, C.L. Bianchi, C. Pirola, S. Vitali, G. Cerrato, S. Morandi, C. Argirusis, G. Sourkouni, P.M. Sakkas, V. Capucci, Surface decoration of commercial micro-sized $TiO_2$, Appl. Catal. B: Environ. 178 (2015) 124–132.

[29] P.J.A. Borm, D. Robbins, S. Haubold, T. Kuhlbusch, H. Fissan, K. Donaldson, R. Schins, V. Stone, W. Kreyling, J. Lademann, J. Krutmann, D. Warheit, E. Oberdorster, The potential risks of nanomaterials: a review carried out for ECETOC, Part. Fibre Toxicol. 3 (11) (2006), http://dx.doi.org/10.1186/1743-8977-3-11.

[30] C.M. Sayes, A.M. Gobi, K.D. Ausman, J. Mendez, J.L. West, V.L. Colvin, Nano-C60 cytotoxicity is due to lipid peroxidation, Biomaterial 26 (2005) 7587–7595.

[31] G. Oberdörster, E. Oberdörster, J. Oberdörster, Nanotoxicology: an emerging discipline evolving from studies of ultrafine particles, Environ. Health Perspect. 113 (2005) 823–839.

[32] E. Bermudez, J. Mangum, B. Wong, B. Asgharian, P. Hext, D. Warheit, Pulmonary responses of mice, rats, and hamsters to subchronic inhalation of ultrafine titanium dioxide particles, Toxicol. Sci. 77 (2004) 347–357.

[33] W. Liu, Y. Xu, W. Zhou, X. Zhang, X. Cheng, H. Zhao, S. Gao, L. Huo, A facile synthesis of hierarchically porous $TiO_2$ microspheres with carbonaceous species for visible-light photocatalysis, J. Mater. Sci. Technol. 33 (2017) 39–46.

[34] D.L. Costa, R.S. Leite, G.A. Neves, L. Navarro de Lima Santana, E.S. Medeiros, R.R. Menezes, Synthesis of $TiO_2$ and ZnO nano and submicrometric fibers by solution blow spinning, Mater. Lett. 183 (2016) 109–113.

[35] T. Yi, S. Yang, X. Li, J. Yao, Y. Zhu, R. Zhu, Sub-micrometric $Li_{4-x}Na_xTi_5O_{12}$ ($0 \le x \le 0.2$) spinel as anode material exhibiting high rate capability, J. Power Sources 246 (2014) 505–511.

[36] C.L. Bianchi, C. Pirola, F. Galli, G. Cerrato, S. Morandi, V. Capucci, Pigmentary $TiO_2$: a challenge for its use as photocatalyst in $NO_x$ air purification, Chem. Eng. J. 261 (2015) 76–82.

[37] C.L. Bianchi, S. Gatto, C. Pirola, A. Naldoni, A. Di Michele, G. Cerrato, V. Crocellà, V. Capucci, Photocatalytic degradation of acetone, acetaldehyde and toluene in gas-phase: comparison between nano and micro-sized $TiO_2$, Appl. Catal. B: Environ. 146 (2014) 123–130.

[38] M. Stucchi, C.L. Bianchi, C. Pirola, G. Cerrato, S. Morandi, C. Argirusis, G. Sourkouni, A. Naldoni, V. Capucci, Copper NPs decorated titania: a novel synthesis by high energy US with a study of the photocatalytic activity under visible light, Ultrason. Sonochem. 31 (2016) 295–301.

[39] E.K. Goharshadi, H. Azizi-Toupkanloo, Silver colloid nanoparticles: ultrasound-assisted synthesis, electrical and rheological properties, Powder Technol. 237 (2013) 97–101.

[40] A. Naldoni, C.L. Bianchi, C. Pirola, K.S. Suslickc, Porous $TiO_2$ microspheres with tunable properties for photocatalytic air purification, Ultrason. Sonochem. 20 (2013) 445–451.

[41] C. Pirola, E. Selli, S. Biella, Photocatalytic $NO_x$ abatement: the role of the material supporting the $TiO_2$ active layer, J. Hazard. Mater. 211–212 (2012) 203–207.

[42] D.C. Boffito et al., Sulfated Inorganic Oxides for Methyl Esters Production, Producing Fuels and Fine Chemicals from Biomass Using Nanomaterials, CRC Press, 2013, pp. 137–162.

[43] C.E. Domini, M.B. Álvarez, G.F. Silbestri, G. Cravotto, P. Cintas, Merging metallic catalysts and sonication: a periodic table overview, Catalysts 7 (2017) 121, http://dx.doi.org/10.3390/catal7040121.

[44] D. Wagner, A.V. Naumkin, A. Kraut-Vass, J.W. Allison, C.J. Powell, J.R. Rumble Jr., NIST Standard Reference Database 20, Version 3.4 (web version), http:/srdata.nist.gov/xps/, 2003.

[45] S.W. Gaarenstroom, N. Winograd, Initial and final state effects in the ESCA spectra of cadmium and silver oxides, J. Chem. Phys. 67 (1977) 3500–3506.

[46] K.K. Paul, R. Ghosh, P.K. Giri, Mechanism of strong visible light photocatalysis by $Ag_2O$-nanoparticle-decorated monoclinic $TiO_2$(B) porous nanorods, Nanotechnology 27 (2016) 315703.

[47] S. Gao, Z. Zhang, K. Liu, B. Dong, Direct evidence of plasmonic enhancement on catalytic reduction of 4-nitrophenol over silver nanoparticles supported on flexible fibrous networks, Appl. Catal. B 188 (2016) 245–252.

[48] C. Peng, W. Wang, W. Zhang, Y. Liang, L. Zhuo, Surface plasmon-driven photoelectrochemical water splitting of $TiO_2$ nanowires decorated with Ag nanoparticles under visible light illumination, Appl. Surf. Sci. 420 (2017) 286–295.

[49] M. Faramarzi Nezhad, N. Shahtahmassebi, M. Behdani, Improvement efficiency of thin-film solar cell by plasmonic properties of silver, Optik 127 (2016) 8419–8422.

[50] Y. Cao, P. Du, Y. Qiao, Z. Liu, Z. Sun, Light absorption enhancement of ~100 nm thick poly(3-hexylthiophene) thin-film by embedding silver nanoparticles, Appl. Phys. Lett. 105 (2014), http://dx.doi.org/10.1063/1.4898600.

[51] A. Kubacka, M.J. Muñoz-Batista, M. Ferrer, M. Fernández-García, UV and visible light optimization of anatase $TiO_2$ antimicrobial properties: surface deposition of

metal and oxide (Cu, Zn, Ag) species, Appl. Catal. B: Environ. 140–141 (2013) 680–690.
[52] C. Wang, R. Pagel, J.K. Dohrmann, D.W. Bahnemann, Antenna mechanism and deaggregation concept: novel mechanism principles for photocatalysis, C. R. Chimie 9 (2006) 761–773.
[53] S.B. Rawal, S. Bera, D. Lee, D. Jang, W. In, Lee, Design of visible-light photocatalysts by coupling of narrow band gap semiconductors and $TiO_2$: effect of their relative energy band positions on the photocatalytic efficiency, Catal. Sci. Technol. 3 (2013) 1822–1830.
[54] S.B. Rawal, A.K. Chakraborty, Y.J. Kim, H.J. Kim, W. In Lee, Double-heterojunction structure of $Sb_xSn_{1-x}O_2/TiO_2$/CdSe for efficient decomposition of gaseous 2-propanol under visible-light irradiation, RSC Adv. 2 (2012) 622–630.
[55] G.A. Kumar, M.V.R. Reddy, K.N. Reddy, Structural and optical properties of AgO thin films grown by RF reactive magnetron sputtering technique, in: Advanced Nanomaterials and Emerging Engineering Technologies (ICANMEET), International Conference, 2013.